Classical imaging theory of a micro-lens with super-resolution

Yubo Duan[1, 2], George Barbastathis[2, 3], Baile Zhang[4, *]

[1]*Department of Bioengineering, Faculty of Engineering, National University of Singapore, Singapore 117574, Singapore*
[2]*Singapore-MIT Alliance for Research and Technology (SMART) Centre, Singapore 138602, Singapore*
[3]*Department of Mechanical Engineering, Massachusetts Institute of Technology, 77 Massachusetts Avenue, Cambridge, Massachusetts 02139, USA*
[4]*Division of Physics and Applied Physics, School of Physical and Mathematical Sciences, Nanyang Technological University, Singapore 637371, Singapore*
**Corresponding author: blzhang@ntu.edu.sg*

Received Month X, XXXX; revised Month X, XXXX; accepted Month X, XXXX;
posted Month X, XXXX (Doc. ID XXXXX); published Month X, XXXX

Super-resolution in imaging through a transparent spherical micro-lens has attracted lots of attention because of recent promising experimental results with remarkable resolution improvement. To provide physical insight for this super-resolution phenomenon, previous studies adopted a phenomenological explanation mainly based on the super-focusing effect of a photonic nano-jet, while a direct imaging calculation with classical imaging theory has rarely been studied. Here we theoretically model the imaging process through a micro-lens with vectorial electromagnetic analysis, and then exclude the previously plausible explanation of super-resolution based on the super-focusing effect. The results showed that, in the context of classical imaging theory subject to the two-point resolution criterion, a micro-lens with a perfect spherical shape cannot achieve the experimentally verified sub-100nm resolution. Therefore, there must be some other physical mechanisms that contribute to the reported ultra-high resolution but have not been revealed in theory.

OCIS Codes: 100.6640, 290.0290, 290.4020, 350.3950, 350.5730

A long-standing issue of traditional microscopy is that its resolution is limited to about half of the illumination wavelength as a result of the loss of evanescent waves during wave propagation. To break this resolution limit and achieve super-resolution, researchers have developed various approaches. One approach is to recover the evanescent waves in far-field by using negative refractive index metamaterials, which could achieve unlimited resolution in theory [1]. However, because of practical difficulties such as loss, this approach has not been practically used. Another approach is to deliberately create a specific situation where only a single light emitting spot (or sparsely distributed spots) will locate in the field of view, such that the overlapping of Point Spread Function (PSF) will not occur in principle. Typical examples include Stimulated Emission Depletion (STED) microscopy and Stochastic Optical Reconstruction Microscopy (STORM) [2]. Although being very successful in practice, these microscopy technologies share an inherent drawback: they generally require temporal and spatial scanning which will take a long time, and thus are not very suitable for dynamic real-time imaging.

Achieving super-resolution without utilizing either evanescent waves or scanning is obviously in great demand. Recently, the phenomenon of photonic nano-jet with a subwavelength focus formed by a transparent micro-lens has been considered as a potential approach to beat the diffraction limit [3-5]. A remarkable record of 50nm lateral resolution has been reported for real-time imaging through a dielectric micro-lens with white light illumination [6]. This significant progress undoubtedly will bring out a profound impact on related disciplines in biology, chemistry, medicine and semiconductor industry. However, the previous attribution of this high resolution [6] to the photonic nano-jet focusing phenomenon [3-5] remains elusive in the sense that imaging and focusing are two distinctive physical phenomena that do not always have necessary connection in resolution. While most previous literatures adopted focusing analysis [6], a direct imaging calculation through a micro-lens with vectorial electromagnetic analysis can provide more physical insights. Here we apply the classical Mie scattering theory to simulate the real imaging process by placing light emitters behind the micro-lens and observing them in the far field.

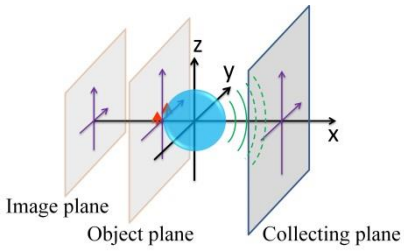

Fig. 1. (Color online) Configuration of image reconstruction of two incoherent dipoles. The origin of the coordinates x-y-z coincides with the center of the micro-lens.

As shown in Fig. 1, two incoherent dipoles pointing in the z direction are placed on the object plane just beside the micro-lens (diameter $D = 4.74$ μm, refractive index $n = 1.46$), similar to the experimental setup of the micro-lens imaging system [6]. The waves radiated from the dipoles propagate through the micro-lens and are collected on the collecting plane in the far-field. The interaction between the dipole radiation and the micro-lens is calculated by multipole expansion based on spherical harmonics and Mie scattering theory. The Numerical Aperture (NA) with respect to the origin of the object plane is 0.9, the same as

in [6]. According to angular spectrum representation, the collected waves are decomposed into plane waves, which will then numerically propagate backward in the negative x direction to form a virtual image on the image plane.

Whispering gallery mode (WGM) excited in a spherical micro-lens has been reported to enhance the resolution [7] since WGM enhances coupling evanescent waves into the micro-lens and converting to propagating waves. To investigate the WGM of the micro-lens in the visible spectrum, we first numerically scan the backward scattering cross section of the micro-lens from wavelength 400nm to 700nm. The first WGM appears at the wavelength 401.64nm. Another wavelength 403.07nm without WGM is chosen for comparison. By placing a single dipole just beside the micro-lens (Fig. 2), we find that the fields at wavelength 401.64nm with WGM (Fig. 2a) are enhanced significantly compared to that at wavelength 403.07nm without WGM (Fig. 2b).

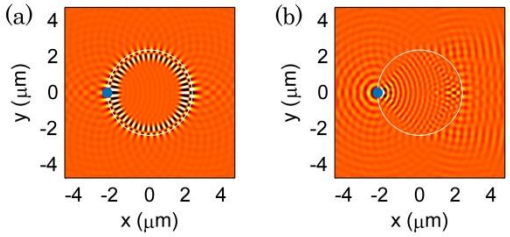

Fig. 2. (Color online) Snapshots of wave propagation in x-y plane for (a) $\lambda = 401.64\text{nm}$ and (b) $\lambda = 403.07\text{nm}$ respectively. The white circle denotes the contour of the micro-lens. The small blue dot denotes the position of the dipole.

To determine the position of the image plane, we examine the reconstructed intensity distribution in the x-y plane, as shown in Fig. 3a and c for wavelengths 401.64 nm and 403.07 nm, respectively, with the single dipole behind the micro-lens. From the view of geometrical optics, the focus of a micro-lens is at $R \times n/(n-2)$ (R is the radius of the micro-lens and n is its refractive index), i.e. at $x = -6.41\mu\text{m}$. This estimation may be applicable to the wavelength 403.07nm without WGM (Fig. 3c), but not appropriate for the wavelength 401.64nm with WGM (Fig. 3a). Alternatively, the maximum intensity position in the x axis ($x = -4.40\mu\text{m}$ for wavelength 401.64nm and $x = -6.84\mu\text{m}$ for wavelength 403.07nm) can be considered as the focus, since the dipole is known to be on the x axis. However, at $x = -4.40\mu\text{m}$ for the wavelength 401.64nm, the maximum side-lobes are 40% of the main-lobe (Fig. 3b), which will cause distortion and poor contrast in wide-field imaging [8]. To reduce side-lobes, the focus $x = -4.87\mu\text{m}$ adopted from [6] is also considered, where the maximal side-lobes decrease to about 22% of the main-lobe. Note that at the position $x = -3.94\mu\text{m}$, the side-lobes are even higher than the main-lobe, which may introduce artifacts in practice.

The Full Width at Half Maximum (FWHM) is a widely used evaluation of resolution. To compare FWHM at different image planes, the magnification of the micro-lens must be considered, although the resolution is not necessarily related to magnification but rather wave coupling and conversion. The magnification can be estimated by shifting the dipole 50nm away from its original position along the y axis and observing the corresponding shift of the virtual image. After being normalized by the magnification (1.82 for 401.64nm at $x = -4.40\mu\text{m}$ and 2.84 for 403.07nm at $x = -6.84\mu\text{m}$), the corresponding effective FWHMs are 107nm (with 40% side-lobes) for wavelength 401.64nm and 214nm for wavelength 403.07nm. The effective FWHM without WGM is close to the diffraction limit in air, while the one with WGM is much narrower, similar to the conclusion in [7]. Note that the effective FWHM with WGM is much smaller than 157nm, the FWHM achievable with an oil immersion lens of the same refractive index 1.46 and angular aperture ($\sin\alpha = 0.9$), which is mainly attributed to apodization. However, significant side-lobes may lead to large distortion and poor contrast in wide-field imaging. The side-lobes caused by apodization may be suppressed in confocal microscopy, where the resolution of a micro-lens can be enhanced by WGM to beat the diffraction limit. In the following text for monochromatic light, only waves with WGM will be considered to explore the possibly highest resolution.

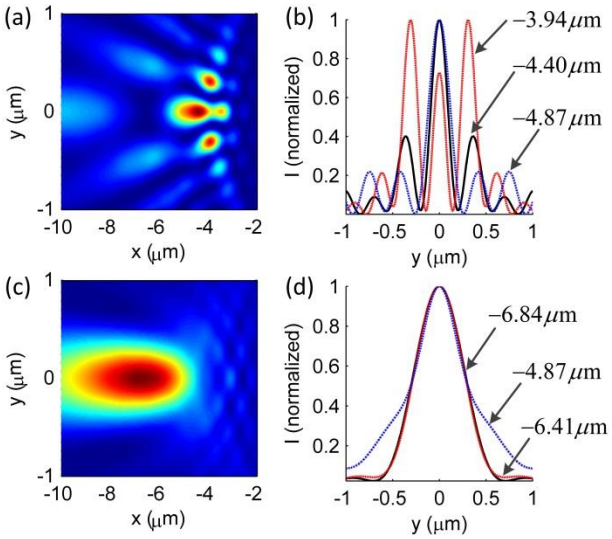

Fig. 3. (Color online) Reconstructed intensity distribution in x-y plane for (a) $\lambda = 401.64\text{nm}$ and (c) $\lambda = 403.07\text{nm}$. Normalized intensity profile of (b) $\lambda = 401.64\text{nm}$ focused at $x = -4.87\mu\text{m}$ (blue dash-dot line), $x = -4.40\mu\text{m}$ (black solid line) and $x = -3.94\mu\text{m}$ (red dashed line), and (d) $\lambda = 403.07\text{nm}$ focused at $x = -6.84\mu\text{m}$ (black solid line), $x = -6.41\mu\text{m}$ (red dashed line) and $x = -4.87\mu\text{m}$ (blue dash-dot line).

Another notable phenomenon is that different modes of WGM have different resolution enhancement. Here we compare the first TE mode and the first TM mode appearing at the wavelengths 401.64nm and 405.55nm, respectively. The analysis in Fig. 4 demonstrates that the effective FWHM, after normalized by magnification, of wavelength 405.55nm is 186nm focused at $-8.17\mu\text{m}$ (maximum intensity position), 271nm focused at $-4.25\mu\text{m}$ (the other peak intensity position), 195nm focused at $-6.41\mu\text{m}$ (geometrical focus) and 413nm focused at $-4.87\mu\text{m}$ (position adopted from [6]). Compared with the TE mode, the TM mode has a much larger FWHM for the given radius and refractive index in our model. Other larger wavelengths with TE and TM WGMs result in larger FWHMs than that at 401.64nm.

To better evaluate resolution with the golden criterion of two-point resolution, we put two emitters behind the micro-lens with illumination wavelength 401.64 nm. Fig. 5a and c show the intensity distribution in x-y plane formed by two incoherent dipoles separated by distances of 150nm and 100nm, respectively. The dipoles separated by 150nm are clearly resolved (Fig. 5a and b). However, the dipoles separated by 100nm are hardly resolved (Fig. 5c and d). One may argue that two peaks can be resolved at the position $x=-3.94\mu$m in the case of 100nm separation. However, the position $x=-3.94\mu$m is not the true focus ($x=-4.40\mu$m), and the peaks are because of side-lobes, as illustrated in Fig. 3a.

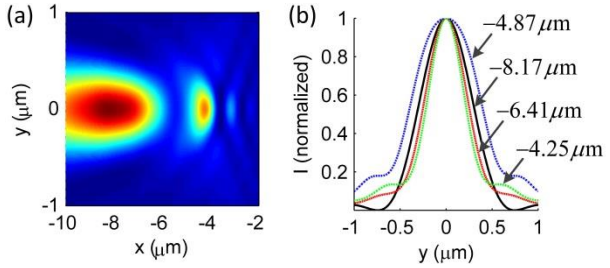

Fig. 4. (Color online) (a) Reconstructed intensity distribution in x-y plane for $\lambda=405.55$nm. (b) Normalized intensity profile focused at $x=-8.17\mu$m (black solid line), $x=-6.41\mu$m (red dashed line), $x=-4.87\mu$m (blue dash-dot line) and $x=-4.25\mu$m (green dashed line).

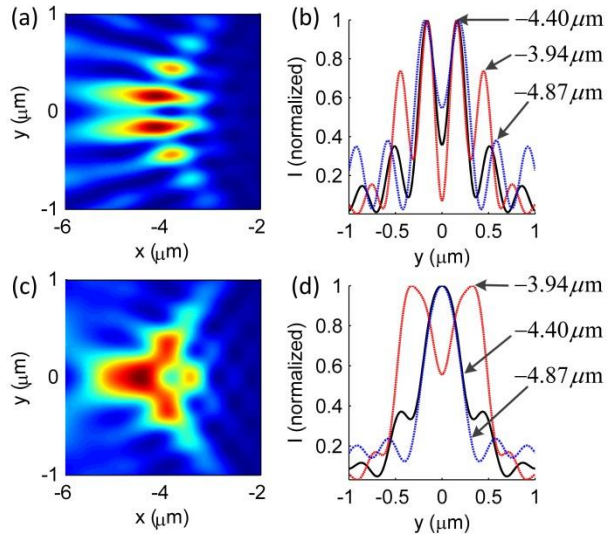

Fig. 5. (Color online) Reconstructed intensity distribution in x-y plane for two incoherent dipoles separated by (a) 150nm and (c) 100nm. Normalized intensity profile for two incoherent dipoles separated by (b) 150nm and (d) 100nm at the focus of $x=-4.87\mu$m (blue dash-dot line), $x=-4.40\mu$m (black solid line) and $x=-3.94\mu$m (red dashed line).

To further explore the resolution of white light illumination, we choose 110 wavelengths including all WGMs in the spectrum 400nm~700nm to mimic white light. With such white light illumination, the micro-lens can resolve two dipoles separated 150nm apart (Fig. 6a), but cannot for those separated 100nm apart (Fig. 6b). Moreover, we have further tested images formed in various focuses, and got almost the same result. Thus, the resolution of a spherical micro-lens with white light illumination cannot reach sub-100nm.

It should be emphasized that in our calculation some realistic factors that have been ignored may offer real reasons for the experimentally observed high resolution in the record. For example, our model only considers perfect spherical shape, while in reality surface roughness may play an important role in near-field imaging. Moreover, the gold-coated fishnet anodic aluminum oxide (AAO) sample was used in experiment [6], but the possible surface plasmon resonance and quantum or nonlocal effects induced by the periodic metallic sample are completely ignored in our calculation.

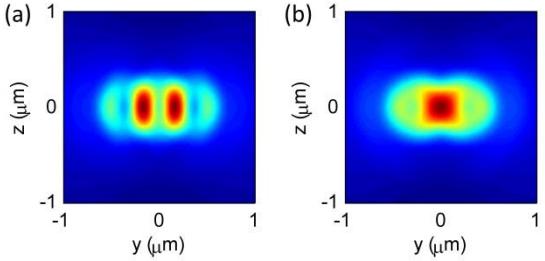

Fig. 6. (Color online) Images formed by two dipoles separated by (a) 150nm and (b) 100nm. The focus is chosen at $x=-4.34\mu$m, where the intensity of the white light is maximal.

In conclusion, the direct imaging process through a micro-lens is calculated with Mie scattering theory. A micro-lens can achieve resolution beyond diffraction limit, but significant side-lobes may cause distortions, poor contrast and even artifacts in wide-field imaging. The resolution of a spherical micro-lens with visible light illumination is between 100nm and 150nm, measured with two-point resolution criterion. Therefore, some important physical mechanisms that have not been revealed (probably surface roughness enhanced surface plasmon resonance, nonlocal effects, or quantum effects) are expected to be involved in the previous successful experiments of ultra-high resolution.

This research was supported by the National Research Foundation Singapore through the Singapore MIT Alliance for Research and Technology's BioSystems and Micromechanics Inter-Disciplinary Research programme, and Nanyang Technological University (M4081153, M4080806).

References

1. J. B. Pendry, Phys. Rev. Lett. **85**, 3966-3969 (2000).
2. H. Wang, C. J. R. Sheppard, K. Ravi, S. T. Ho, and G. Vienne, Laser & Photon. Rev. **6**, 354-392 (2012).
3. X. Li, Z. Chen, A. Taflove, and V. Backman, Opt. Express **13**, 526-533 (2005).
4. J. Y. Lee, B. H. Hong, W. Y. Kim, S. K. Min, Y. Kim, M. V. Jouravlev, R. Bose, K. S. Kim, I. C. Hwang, and L. J. Kaufman, Nature **460**, 498-501 (2009).
5. D. R. Mason, M. V. Jouravlev, and K. S. Kim, Opt. Lett. **35**, 2007-2009 (2010).
6. Z. Wang, W. Guo, L. Li, B. Luk'yanchuk, A. Khan, Z. Liu, Z. Chen, and M. Hong, Nat. Commun. **2**, 218 (2011).
7. A. Heifetz, J. J. Simpson, S.-C. Kong, A. Taflove, and V. Backman, Opt. Express **15**, 17334-17342 (2007).
8. C. Sheppard, Optik **48**, 329-334 (1977).

References

1. J. B. Pendry, "Negative Refraction Makes a Perfect Lens," Phys. Rev. Lett. 85, 3966-3969 (2000).
2. H. Wang, C. J. R. Sheppard, K. Ravi, S. T. Ho, and G. Vienne, "Fighting against diffraction: apodization and near field diffraction structures," Laser & Photon. Rev. 6, 354-392 (2012).
3. X. Li, Z. Chen, A. Taflove, and V. Backman, "Optical analysis of nanoparticles via enhanced backscattering facilitated by 3-D photonic nanojets," Opt. Express 13, 526-533 (2005).
4. J. Y. Lee, B. H. Hong, W. Y. Kim, S. K. Min, Y. Kim, M. V. Jouravlev, R. Bose, K. S. Kim, I. C. Hwang, and L. J. Kaufman, "Near-field focusing and magnification through self-assembled nanoscale spherical lenses," Nature 460, 498-501 (2009).
5. D. R. Mason, M. V. Jouravlev, and K. S. Kim, "Enhanced resolution beyond the Abbe diffraction limit with wavelength-scale solid immersion lenses," Opt. Lett. 35, 2007-2009 (2010).
6. Z. Wang, W. Guo, L. Li, B. Luk'yanchuk, A. Khan, Z. Liu, Z. Chen, and M. Hong, "Optical virtual imaging at 50 nm lateral resolution with a white-light nanoscope," Nat. Commun. 2, 218 (2011).
7. A. Heifetz, J. J. Simpson, S.-C. Kong, A. Taflove, and V. Backman, "Subdiffraction optical resolution of a gold nanosphere located within the nanojet of a Mie-resonant dielectric microsphere," Opt. Express 15, 17334-17342 (2007).
8. C. Sheppard, "The use of lenses with annular aperture in scanning optical microscopy," Optik 48, 329-334 (1977).